HHS Public Access

Author manuscript

J Control Release. Author manuscript; available in PMC 2019 July 28.

Published in final edited form as:

J Control Release. 2018 July 28; 282: 156–165. doi:10.1016/j.jconrel.2018.05.006.

Accelerated wound healing by injectable star poly(ethylene)-*b*-poly(propylene sulfide) scaffolds loaded with poorly water-soluble drugs

Suwei Zhu[1], **Shuoran Li**[1], **Helena Escuin-Ordinas**[2], **Robert Dimatteo**[1,7], **Weixian Xi**[1,8,9], **Antoni Ribas**[2,3,4,5], and **Tatiana Segura**[1,5,6,7,*]

[1]Department of Chemical and Biomolecular Engineering, University of California, Los Angeles, 420 Westwood Plaza, 5531 Boelter Hall, Los Angeles, CA 90095, United States

[2]Department of Medicine, Division of Hematology-Oncology, University of California, Los Angeles, 420 Westwood Plaza, 5531 Boelter Hall, Los Angeles, CA 90095, United States

[3]Department of Surgery, Division of Surgical Oncology, University of California, Los Angeles, 420 Westwood Plaza, 5531 Boelter Hall, Los Angeles, CA 90095, United States

[4]Department of Molecular and Medical Pharmacology, University of California, Los Angeles, 420 Westwood Plaza, 5531 Boelter Hall, Los Angeles, CA 90095, United States

[5]Jonsson Comprehensive Cancer Center, University of California, Los Angeles, 420 Westwood Plaza, 5531 Boelter Hall, Los Angeles, CA 90095, United States

[6]Department of Medicine, Division of Dermatology, University of California, Los Angeles, 420 Westwood Plaza, 5531 Boelter Hall, Los Angeles, CA 90095, United States

[7]Department of Bioengineering, University of California, Los Angeles, 420 Westwood Plaza, 5531 Boelter Hall, Los Angeles, CA 90095, United States

[8]Department of Orthopeadic Surgery, University of California, Los Angeles, 420 Westwood Plaza, 5531 Boelter Hall, Los Angeles, CA 90095, United States

[9]Biomedical Engineering Department, Duke University, Durham, NC

Abstract

Injectable hydrogel matrices take the shape of a wound cavity and serve as scaffold for tissue repair and regeneration. Yet these materials are generally hydrophilic, limiting the incorporation of

*E-mail of corresponding author: tatiana.segura@duke.edu.

Author contributions

S.Z., T.S. and A.R. designed the experiments; S.Z., S.L., H.E-O, RD and WX. performed the experiments; S.Z., S.L. and T.S. analyzed the results and wrote the manuscript.

Competing financial interest

T.S., A.R and H.E-O. declare conflics of interest with Lutris Pharma, which seeks to commercialize technology related to this publication.

poorly water soluble, hydrophobic drugs. Here we show this shortcoming is circumvented through a *star*-shaped amphiphilic block copolymer comprising poly(ethylene glycol) and poly (propylene sulfide). This *star*-shaped amphiphilic polymer self-assembles in an aqueous medium into a physically stable hydrogel and effectively dissolves hydrophobic molecules delivering them at therapeutic doses. The self assembled hydrogel is a robust three-dimensional scaffold *in vivo* effectively promoting cellular infiltration, reducing inflammation, and wound clsoure. When combined with a hydrophobic BRAF inhibitor that promotes paradoxical mitogen-activated protein kinase (MAPK) activation in keratinocytes and wound closure, our self assembled scaffold supported dermal wound closure at a reduced drug dosage compared to administering the drug in dimethyl sulfoxide (DMSO) without a polymeric matrix. This family of *star*-shaped amphiphilic polymers delivers poorly water soluble active agents at a fraction of generally required dosage for efficacy and supports three-dimensional cell growth at tissue wounds, showing great promise for novel uses of hydrophobic drugs in tissue repair applications.

Graphical Abstract

Keywords

Delivery scaffold; hydrophobic drugs; tissue repair

Introduction

The development of injectable scaffolds to promote tissue repair and regeneration has been primarily driven by the need to match the physical and biochemical parameters of a desired anatomical location, while using a minimally invasive implantation procedure. These scaffolds are generally composed of hydrophilic polymers and are optimized to have bulk properties matching those at the intended target site, such as material stiffness and bioactive signals. However, these approaches are limited by their hydrophilicity narrowing the types of active agents that can be incorporated to hydrophilic macromolecules such as peptides and growth factors.

Many small-molecule drugs or drug candidates are hydrophobic compounds, targeting signaling pathways or directly interfering with protein-protein interactions[1]. The use of small-molecule compounds as modulators of tissue repair and regeneration is currently an underutilized resource. A complication of using hydrophobic drugs is that the functional groups imparting specificity in targeting drug-protein interactions[2] are often nonpolar and hydrophobic, thus disfavored in aqueous solubility. For example, Zhang et al. utilized poly(ethylene oxide)-poly(propylene oxide) based hydrogel to entrap microcrystals of drug agents to assess tissue regeneration in adult mice[3]. However, insufficiently solubilized drug candidates may undergo crystalization and cause acute toxicity.[4] To circumvent this

problem, previous studies have developed carriers such as micelles[5–7], micro-/nanospheres[8], emulsion gels/creams[9, 10] and film[11]/patches. In the former two strategies, amphiphlic polymers permits the dissolution of hydrophobic drugs in an injectable vehicle for tissue surface distribution of therapeutics,[6, 12] but the form of particulates lacks a macroscopic structure to support cell infiltration and tissue remodeling in a tissue cavity. Emulsion gels from ABA block copolymers of PLGA-PEG-PLGA result in thermal gelation polmers that solidify at body temperature and can be used to solublize hydrophobes. However, the resulting gels are not suitable as scaffolding materials since they contain a high amount of surfactants[13]. Other, reverse thermal gelation block co-polymers such as poloxamers or their equivalents incorporate hydrophobes through micellar structure in aqueous media, but linear structures and short-range molecular interactions often require excessive polymer concentrations (e.g., 25 w/v% or higher) to increase stability *in vivo*, but the incorporated drugs easily elute off in a matter of hours[14]. Alternatively, hydrophobic scaffolds support extended drug release via simple diffusion and polymer degradation[15]. A non-covalently associated polymer-nanoparticle hydrogel supported an improved two-stage drug release profile, but it requires separate preparation of nanoparticles besides gel formation and selective adsorption of certain biopolymers[16]. Other scaffolds such as poly(ether urethane) and cyclodextrin provides for oxidation responsiveness[17, 18], but the abilities to solubilize hydrophobes and maintain structural integrity are unclear.

Here we demonstrate an amphiphilic *star*-shaped block copolymer that self-assembles into a stable hydrogel *in vivo* for tissue regrowth and solubilizes hydrophobic agents for therapeutic dosing at an reduced amount. A one-step approach combining polymer network assembly and solubilization of hydrophobes allows the formation of injectable hydrogel amenable to mechanical manipulation (*e.g.*, injectability) and alterations in response to biochemical changes (*e.g.*, redox responsiveness). Previously, a linear ABA block copolymer of poly(ethylene glycol)-poly(propylene sulfide)- poly(ethylene glycol) (PEG_{16}-*b*-PPS_{50}-*b*-PEG_{16}) formed oxidation-responsive micelles for drug delivery[19]. Branched, four-arm block copolymer of poly(ethylene glycol-polypropylene sulfide) (*star*-PEG_{113}-PPS_5) was found to support cell cultivation *in vitro* and serve as a vehicle for stem cell transplantation to the stroke cavity *in vivo* [20]. Here, *star*-PEG_{113}-PPS_x, coupled with an integrin-binding, cell adhesive peptide based on an amino acid sequence of RGD, provides a self-assembling injectable hydrogel capable of incorporating hydrophobic agents. In particular, a hydrophobic BRAF inhibitor that promotes paradoxical mitogen-activated protein kinase (MAPK) activation in keratinocytes and wound closure [21] was delivered. Our self assembled scaffold supported dermal wound closure at a reduced drug dosage compared to administering the drug in dimethyl sulfoxide (DMSO) without a polymeric matrix.

Experimental Section

Synthesis of PEG-PPSx:

The synthesis of PEG-PPS follows a three-step reaction, primarily described in previous publication with slight modifications.[22] Briefly in the first step, 10 g four-arm poly(ethylene glycol) (PEG) (MW 20,000, 2 mmol arms; A starting material of 20,000 dalton, four-arm PEG was used, each arm having approximately 113 repeating units of

ethylene glycol)) was dissolved in 120 mL dried tetrahydrofuran (THF) (pretreated with activated molecular sieves for overnight) and refluxed under argon gas at 90 °C for 4 hours. After the flask was cooled down, 0.6 g sodium hydride (8x excess over arms =16 mmol) was slowly added to the dissolved PEG and stirred for 15 min under argon. Subsequently 1.6 mL allyl bromide (10x excess over arms = 20 mmol) was injected into the mixture and the reaction was stirred under argon for overnight. To purify the reaction product of PEG-allyl ether, the reaction mixture was filtered under vacuum and the filtrate was dried to remove excess solvent. The viscous sample was redissolved in a small amount of dichloromethane and precipitated out in 200 mL ice-cold ethyl ether for two times. The precipitant was collected and dried under vacuum for overnight and subsequently stored in argon at −20 °C. NMR was used to characterize the final sample for modification. [23] ^{1}H NMR (400 MHz, $CDCl_3$): 3.39–3.89 (broad, PEG chain protons), 5.85–5.98 (m, 1H, -$CH_2OCH_2C\mathbf{H}=CH_2$), 5.15–5.30 (m, 2H, -$CH_2OCH_2CH=C\mathbf{H}_2$).

Second, PEG-allyl ether (3.78 g, 0.73 mmol arms) was dissolved in 130 mL anhydrous toluene with stirring and warming below 45 °C in a schlenk tube. The solution subsequently underwent freeze-pump-thaw degassing cycles until no bubbles were seen in the thawing step. The radical initiator 2,2′-Azobis(2-methylpropionitrile) (AIBN) (1.5 g, 9 mmol) was freshly activated via recrystallization in methanol. Recrystalized AIBN and 2 mL thioacetic acid (26 mmol) dissolved in 20 mL anhydrous toluene were added to PEG-allyl ether solution in five aliquots over one day. The reaction was carried out at 80 °C for 72 hours in argon with aliquots of AIBN/thioacetic acid added at an interval of 2–3 hours. The reaction product of PEG-thioacetate was dried and precipitated in ice-cold ethyl ether. NMR was used to characterize the final sample for modification. ^{1}H NMR (400 MHz, $CDC1_3$): 1.81–1.9 (q, 2H, - $OCH_2C\mathbf{H}_2CH_2S$-), 2.35 (s, 3H, -$SCOC\mathbf{H}_3$), 2.92–2.97 (t, 2H, -$OCH_2CH_2C\mathbf{H}_2S$-), 3.39–3.89 (broad, PEG chain protons).

Third, PEG-thiolacetate (0.78 g, 0.153 mmol arms) was dissolved in freshly distilled THF. Sodium methoxide (83 mg, 10x excess over arms = 1.53 mmol) was added to PEG-thiolacetate/THF under argon and stirred for 30 min at room temperature. Subsequently specific amounts of propylene sulfide (2.5x, 5x and 16x molar equiv. of PEG arms) was added under argon and the reaction mixture was stirred for one hour. The end-capping reagent 2,2,-dithioldipyridine (168 mg, 5x excess over arms = 0.77 mmol) was later added and the reaction mixture was stirred under argon for overnight. The sample of PEG-PPSx was later dried via rotary evaporator and dialyzed extensively against water. Lastly, the sample was lyophilized and stored under argon at −20 °C. NMR was used to characterize the final sample for modification. ^{1}H-NMR (in $CDCl_3$): 1.35–1.45 (d, CH3 in PPS chain), 1.81–1.9 (broad q, 2H, -$OC\mathbf{H}_2CH_2CHS$), 3.6–3.7 (broad PEG chain protons).

Rheometry:

PEG-PPS hydrogels were allowed to self-assemble overnight before transferred to an 8 mm plate-to-plate rheometer (Physica MCR 301, Anton Paar, Ashland, VA). An evaporation blocker system was used during measurements. For frequency sweep, the data were collected for the modulus with a frequency range of 0.1–100 rad/s under a 1% constrain at

37 °C. For amplitude sweep, the data were collected for the modulus with a frequency of 20 rad/s under a constrain range of 0.1–100% at 37 °C.

Water content measurements:

Hydrated self-assembled PEG-PPS hydrogels were weighed for the wet mass (W_{wet}). Subsequently they were stored in a vacuum oven for two days until the mass did not change. The dried polymers were weighed (W_{dry}). Water content (%) was calculated as (W_{wet} - Wdry)/Wwet*100%.

Oxidation of PEG-PPS:

The reduction modification on PEG-PPS was performed in two steps. The first step was to use Ellman's assay (following manufacturer's instructions) to determine all the available thiol groups on a certain percentage of aqueous solution of PEG-PPS. The second step was to use different amounts of TCEP to treat PEG-PPS, resulting in various degrees of disulfide-crosslinked PEG-PPS (confirmed by Ellman's assay).

Fluorescent labeling of star-PEG-PPS:

6 mg *star*-PEG-PPS was dissolved in 100 μL 1x PBS and mixed with 2 μL TCEP (10 mg/ml) solution for 1 hour. Then 8.6 μL of Alex-488-maleimide (1 mg/mL) was added to the solution, and the mixture was vortexed at room temperature overnight. The solution was diluted with 500 μL 1x PBS and then dialyzed against DI water with MWCO 10000 membrane for two days. After dialysis, the solution was lyophilized to get the solid product. For the *in vivo* experiment, 5 mg of Alex-488 labeled *star*-PEG_{113}-PPS_5 was assembled in 100 μL sterile 1x PBS for administration.

Solubilization of hydrophobic molecules

A 4 w/v% polymer (*star*-PEG-PPS_5) solution of was mixed with a hydrophobe by vortexing at room temperature for 30 minutes. Serial dilutions of the hydrophobe were performed until no obvious precipitate or crystals were observed via phase contrast microscopy. The maximum concentration that could be dissolved is reported. Images were taken using a Zeiss Observer Z1 microscope at 5x magnification.

Delivery of hydrophobic molecules at wound site:

Animal procedures were performed in accordance with the Animal Protection Guidelines issued by US National Institutes of Health. UV sterilized PEG-$PPS_{2.5}$ (at 10 w/v%) and PEG-PPS_5 (at 6 w/v%) were incubated with 500 μM Acetyl-GCGYGRGDSPG-NH_2, an adhesive peptide (RGD) containing a Cystein amino acid, and BrdU (at 10 mg/mL) in sterile phosphate buffer saline for overnight. The excisional splinted wound protocol was an established protocol previously reported by others and in details by our previous publication. [24] Briefly, young adult (7–12-week old mice) (Charles River Laboratories) were acclimated to the environment for at least 1 week upon delivery prior to the procedure. Mice were individually anesthetized with 4% isoflurane and maintained at 1.5–2% isoflurane during surgery. Buprenorphine (fours dosages of 60 uL each of 0.015 mg/mL per 20 g of mouse weight administered before, 8 hours, 20 hours and 28 hours after surgery) was

injected subcutaneously. Buprenorphine is a well-documented commonly used analgesic in mice. The dorsal surface was shaved with an electric clipper, depilated by Nair (1 minute) and sterilized with betadine and ethanol before surgery on an aseptic pad atop warming heat pads. Using sterile biopsy punches (1) 4 mm wide for the experiment delivering BrdU; or (2) 6 mm wide for the experiment delivering Vemurafenib, two clean, well-defined wounds side-by-side were created slightly above the middle of the animal's back. Bromodeoxyuridine (BrdU), a synthetic nucleoside analog of thymidine, was first tested. It is incorporated within newly synthesized DNA to effectively label dividing cells. During wound healing, collective migration of cells is primarily wound directed, so any diffusion of BrdU from *star*-PEG-PPS hydrogel would allow proliferating cells at wound periphery or beyond to uptake BrdU. To account for the differences in cell proliferation in different wounds, another general proliferating cell marker, Ki-67, was used to gauge such difference and to normalize BrdU+ cells in the analysis of BrdU diffusion. The number of proliferating cells as labeled by BrdU-positive cells, normalized by Ki-67-positive cells, indicates a relative amount of available BrdU at a certain wound region. We hypothesized that a longer hydrophobic block enhances retention of BrdU, thus less normalized BrdU-positive cells would be noticeable farther away the injected gel. (1) For the experiment delivering BrdU, PEG-$PPS_{2.5}$ hydrogel and PEG-PPS_5 hydrogel containing BrdU were injected on wounds; Aseptic silicon ring splints formed prior to surgery had a 6-mm wide window that was double-sided with Tegaderm. (2) For the experiment delivering Vemurafenib (VEM), 150 μg VEM mixed in 50 μl of 40 mg/mL PEG-PPS_5 aqueous hydrogel, or 50 μl of 40 mg/mL PEG-PPS_5 aqueous hydrogel alone, was injected on wounds; Aseptic silicon ring splints formed prior to surgery had a 8-mm wide window that was double-sided with Tegaderm. Mastisol liquid adhesive was added on the splints which were placed on a wound. Eight interrupted sutures around each splint were made as a secondary means to hold down splints. Animals were monitored until awakening and housed individually in cages. (1) For the experiment delivering BrdU, on day 3 and day 7 post surgery, or (2) for the experiment delivery VEM, on day 14 post surgery, animals were euthanized and wounded tissues were punched out and cut in halves, where one half was fixed with 1% paraformaldehyde (PFA) for 16–18 hours at 4°C before paraffin embedding and the other half was freshly frozen in Tissue-Tek® O.C.T. Compound. Paraffin sections were sliced into 5 μm thickness, for the experiment delivering Brdu, or 4 μm for the experiment delivering VEM, for hematoxylin and eosin (H&E) stain. Cryo sections of skin cross-sections were sliced as 20 μm for immunohistochemistry staining. Animals were assigned randomly and all tissue analysis was performed in a blind manner.

Immunohistological analysis:

(1) For the experiment delivering BrdU, the primary antibodies used included rat anti-CD31 (1:100), rabbit anti-NG-2 (Millipore, 1:100), rat anti-F4/80 (eBioscience, 1:100), rat anti-BrdU (Abcam, 1:100), rabbit anti-Ki 67 (1:100). Alexa Fluor conjugated matching secondary antibodies (1:200, Life Technologies) were used. Three slides (50~100 μm apart) and each with designated fields of view (Region I, II, III for wound center, wound/granulation tissue, and normal wounds) were imaged using a Nikon C2 confocal microscope. A full wound scan was also performed. Images were quantified in Image J for positive signal areas and averaged across four different wounds for statistical analysis.

(2) For the experiment delivering VEM, paraffin-embedded slices of wound tissue was deparaffinized with xylene and descendant ethanol, and then incubated in 3% H_2O_2 for 10 minutes. After a wash in distilled water, the slides were incubated for 25 minutes in Citrate Buffer pH6 (Invitrogen Corporation) at 95 °C using a vegetable steamer. The slides were brought to room temperature, rinsed in PBST (Phosphate Buffered Saline containing 0.05% Tween-20), and then incubated at room temperature with 1:100 anti-mouse Ki-67 antibody (DAKO, Carpinteria, CA) for 1 hour and 1:10 phospho-ERK Ab (Cell Signaling Technology, Danvers, MA), overnight. The Ki67 stained slides were rinsed with PBST and incubated at room temperature with 1:200 polyclonal Rabbit anti-rat immunoglobulin/ Biotinylated Ab (Dako, E0468) for 30 minutes. All the slides were rinsed with PBST, and incubated with Dako EnVision+ System -HRP Labelled Polymer Anti-Rabbit (Dako, Carpinteria, CA) at room temperature for 30 minutes. After a rinse with PBST, the slides were incubated with DAB (3,3,-Diaminobenzidine) for visualization. Subsequently, the slides were washed in tap water, counterstained with Harris, Hematoxylin, dehydrated in ethanol, and mounted with media. The imaging and quantification of our cell-based immunohistochemistry, was performed with the Halo Next Generation Imaging analysis software (Indica Labs; Corrales, NM). HALO measures and reports individual cell data maintaining an interactive link between cell metrics and cell imagery. The number of pERK + or Ki67+ cells was automatically counted with the Halo software. pERK+ or Ki67+ cells were automatically counted on the 3mm whole wound (include both left and right 1.5 mm range from the wound center). For cryo-embedded slices of wound tissue, the slices were fixed in ice-cold acetone for 5 min, washed with 1XPBS for 5 min before blocked for 1 hr at room temperature in blocking buffer: 1XPBS + 0.05% Tween-20 + 5% normal goat serum. Sections are then washed in 1XPBST. Primary antibodies were prepared in blocking buffer, including rabbit anti-mouse Keratin 14 (Biolegend; #905301; 1:200), mouse α-SMA-FITC (Sigma; #F3777; 1:200), rabbit anti-mouse collagen 1(Millipore; #AB765P; 1:200), rat anti-mouse CD31 (BD Pharmingen; #553370; 1:100), and rabbit anti-mouse NG2(Millipore; #AB5320; 1:200). Sections were stained with primary antibodies overnight, then were washed with 1XPBST twice, then re-incubated with blocking buffer for 10 min before secondary antibody incubation. Secondary antibodies were all prepared at a dilution of 1:200 in blocking buffer together with 2 μg/mL DAPI. Sections were then incubated in secondary antibodies for 2 hours at room temperature, and subsequently washed with 1X PBST and 1XPBS. Sections were mounted in Antifade Gold mounting medium. Imaging was performed using a Nikon C2 confocal and images were analyzed using Image J.

Statistical analysis:

All in vitro characterizations were compared for n = 3, and in vitro characterizations for n = 4. One-way ANOVA analysis was performed with Tukey's post test, * $p<0.05$, ** $p<0.01$, *** $p<0.001$.

Results and Discussion

From star amphiphilic block copolymers to stable injectable hydrogel networks

A *star-shaped* polymer architecture contains a poly(eythylene glycol) center and poly(propylene sulfide) ends, which interacts with one another in an aqueous medium based

on physical bondings including hydrophobic interactions and hydrogen bonding. A family of *star*-PEG_{113}-PPS_x polymers was prepared with increasing hydrophobic domain sizes (Figure 1a). NMR analysis confirmed the synthesis of *star*-PEG_{113}-b-PPS_x containing three different lengths of the hydrophobic block, namely *star*-PEG_{113}-$PPS_{2.5}$, *star*-PEG_{113}-PPS_5 and *star*-PEG_{113}-PPS_{16} (Supplementary Figure S1). The length of hydrophobic block in the *star* polymers was modulated to vary the viscoelasticity of the self-assembled structures. While *star*-PEG_{113}-$PPS_{2.5}$ was in a liquid-like state when solvated in water, *star*-PEG_{113}-PPS_5 and *star*-PEG_{113}-PPS_{16} were in a gel state (Figure 1b, c). When solvated in methanol, *star*-PEG_{113}-$PPS_{2.5}$ immediately solubilized, whereas *star*-PEG_{113}-PPS_5 and *star*-PEG_{113}-PPS_{16} were elastic by rheology (Figure 1b, c). Therefore, increasing PPS block length results in a stronger physical interactions between the hydrophobic domains, thereby increased hydrophobic-hydrophilic segregation leading to stiffer gels. Although longer PPS domains increased hydrogel stability and hydrophobic content, *star*-PEG_{113}-PPS_{16} solubilized slowly in water and was difficult to work with in an aqueous environment. *star*-PEG_{113}-PPS_5 was readily solvated in aqueous solutions and the formed hydrogel remained semi-transparent microscopically, having a water content over 90 w/w % (Supplementary Figure S2).

Formed through self-assembly, *star*-PEG_{113}-PPS_x hydrogels were expected to exhibit shear-thinning and self-healing properties, desirable for injectability. First, the hydrogel storage and loss modulus were evaluated at low oscillation frequencies (0.1 to 50 s^{-1}). The average storage moduli (G') for 3, 5, 7.5, and 10 w/v% polymer contents were 35, 270, 907, and 1850 Pa, respectively (Figure 1d and Supplementary Figure S3), all greater than respective viscous moduli (G"). At all concentrations the hydrogels exhibited a time (frequency)-dependent shear thinning property, i.e., at low frequencies the polymer solution behaves as a solid (G'>G") but at high frequency the polymer solution behaves as a liquid (G" > G') (Figure 1e and Supplementary Figure S4). Additionally the hydrogel exhibited a selfhealing behavior after cessation of shear forces. As the oscillatory deformation increased from 0.1 to 100 percent at a constant frequency, *star*-PEG_{113}-*b*-PPS_5 yielded (i.e., G' = G") at strains 33 ± 4 %, 27 ± 6%, and 20 ± 8% for 5, 7.5, and 10 w/v% polymeric concentrations, respectively ($p = 0.11$). Repeatedly, as shear deformation re-started at 0.1%, elastic state (G'>G") was maintained until yielding at the mentioned threshold strains where the solution turned into a viscous state (G'<G"). This yielding behavior was previously observed in other systems where the polymer "breaks" (flows) under high shear force and "heals" (gels) once the shear force ceased.[25]

Reducing and oxidative stimuli are expected to be present in biological systems such as in wound environmens [26]. This oxidation responsive property was previously shown to mediate drug release from micelles formed with propylene sulfide as the hydrophobic block, which are oxidizable to become sulfones [19, 20]. Here we validated *star*-PEG_{113}-PPS_5 hydrogel underwent oxidation dissolution in the presence of hydrogen peroxide, decreasing the viscosity of the polymeric network (Figure 1g). Additionally, we showed *star*-PEG-PPS hydrogel is reduction-responsive through the end-capping group of pyridinethion. This group provides for a disulfide bridge at the end of propylene sulfide blocks. Upon addition of a thiol reducing agent such as tris(2-carboxyethyl)phosphine (TCEP) to a 4.75 *% star*-PEG_{113}-PPS_5, sulfhydryls are exposed and allow for disulfide exchange reactions with other end-capped PPS blocks. This results in a disulfide covalent bond between adjacent polymer

chains and further stiffens gel network. When 0.5x equivalence of TCEP to the total amount of polymer arms was added, the elastic moduli of *star*-PEG_{113}-PPS_5 hydrogel increased from 100 Pa to 300 Pa (Figure 1f). As is shown previously [20], upon incubation at physiological pH, the *star*-PEG-PPS hydrogels become covalently crosslinked due to disulfide exchange reactions between the propylene sulfid units. Thus, the physiological pH, any reducing agent, or a combination of both *in vivo*, allow for a gradual stiffening of the gel to transition from a viscous fluid to a viscoelastic hydrogel. This is also expected to slow down the drug release therefrom. Consequently, as a result of being oxidized, the gel is expected to soften and microscopically dissolute in regions where drug dosing would be wuickened.

Injectable star PEG-PPS hydrogels as biocompatible, stable scaffolds for tissue repair

Given the injectability of *star*-PEG_{113}-PPS_x hydrogels and oxydation responsive properties of polypropylene sulfide, we hypothesized that *star*-PEG-PPS hydrogels could be used as an effective injectable scaffold that promotes wound healing through promoting cellular infiltration and reducing inflammation through sequestering reactive oxygen species. Splinting the wounds in mice prevents loose skin contraction, thereby allowing for assessment of tissue healing through re-epithelialization and granulation, which simulates the response in humans and fixed-skinned mammals[24]. *Star*-PEG-PPS hydrogel was directly injected at the wound site to fill the cavity due to its shear-thinning, self-assembly property. Prior to injection, *star*-PEG-PPS polymer was modified with an RGD-containing peptide via the disulfide exchange reaction at the end group to promote spreading and proliferation of cells in PEG-PPS hydrogels [20]. Two *star*-PEG-PPS polymers sharing a similar viscoelastic property, i.e., 10 w/v% *star*-PEG_{113}-*b*-$PPS_{2.5}$ and 6 w/v% *star*-PEG_{113}-*b*-PPS_5, were individually administered to excisional skin wounds before splinting (Figure 2a). For comparison, a 1 w/v% fibrin gel was formed *in situ* at the wound site. The wounds treated with *star*-PEG-PPS polymer gels displayed enhanced wound closure at day 3 compared to fibrin treated wounds (Figure 2b). Histological analysis performed at day 7 confirmed injectable *star*-PEG-PPS_5 hydrogel allowed for cellular infiltration and supported tissue growth in the scaffold (Figure 2c). Fluorescent imaging confirmed that fluorescently labeled *star*-PEG-PPS_5 was retained as a scaffold structure at day 7 post injection in the cutaneous wound (Figure 2d), which did not erode or wear off. In addiiton, similar to the hystological stains cellular infiltration was observed (Figure 2e, insets 1 and 2). Compared with fibrin, *star*-PEG_{113}-PPS_5 treated wounds had statistically lower fraction of lymphocyte antigen 6 complex locus G6D (Ly6G)-positive cells, e.g., cells of the myeloid lineage such as neurophils responsible for early tissue inflammation[27], at day 7 (Figure 2e,f), suggesting a sustained lower inflammatory response. This finding is consistent with our expectation that polypropylene sulfide's oxydation responsive properties [19] act as a reactive oxygen species (ROS) quencher in inflammaed wounds [28]. Given that 2.5 units of polypropylene sulfide does not statistically improve healing nor reduce Ly6G positive cells in the wound area, we hypothesize that there is a critical number of polypropylene sulfide units required to observe anti-inflammatory properties, which is higher than 2.5 and lower or equal to 5. Reduced Ly6G positive cells has been shown to enhance cutaneous wound healing[29] and excesive neurophil count is associated with diabetic wounds[30], which is consistent with our findings of enhanced wound closure for *star*-PEG_{113}-PPS_5 (Figure 2b).

Hydrophobic drug solubilization and retention at wound sites

Current approaches to topically delivering hydrophobic drugs such as chemotherapeutic agents generally utilize an organic medium[31, 32] or insolube polymeric micro or nanoparticles[33]. We hypothesized hydrogel formed from *star*-PEG-PPS can solubilize hydrophobic agents, providing a facilely-prepared drug-loaded tissue scaffold for wound repair. *Star*-PEG_{113}-PPS_x was able to solublize rifampicin (reported logD = 1.28; from Cerep, FR, Application Notes July 2013), eosin Y (reported partition coefficient 0.66 [34]), Irgacure® 2959 (reported logP = 0.84; from Safety Data Sheet, BASF), and vemurafenib in *star*-PEG_{113}-*b*-PPS_x, whereas they would remain largely insolubilized in distilled water at room temperature even after vibrant vortexing for 1 day (Figure 3a; Supplementary Figure S5). Solubilization of the hydrophobes was achieved at least at a 4 w/v% polymer concentration by simply mixing the polymer solution with the hydrophobe by vortexing. Since the polymer is a gel at these concentrations, the incorporation of poorly water-soluble drugs into *star*-PEG_{113}-b-PPS_x hydrogels is a a one-step process, making it an ideal platform for the injectable delivery of hydrophobes within a polymeric matrix.

We next explored the idea that drug-loaded self-assembled PEG-PPS hydrogels retain hydrophobic drugs locally and avoid uncontrolled elution, while supporting cell infiltration. To compare the efficacy of retaining hydrophobic drugs *in vivo, star*-PEG_{113}-$PPS_{2.5}$ and *star*-PEG_{113}-PPS_5 sharing similar viscoelastic properties as previously identified were used to deliver bromodeoxyuridine (BrdU) to cutaneous wounds. BrdU is a synthetic nucleoside analog of thymidine, which is incorporated within newly synthesized DNA to effectively label dividing cells. Similar to other hydrophobes, BrdU was not entirely solubilized by either water or an aqueous fibrinogen solution even after vortexing at room temperature for 1 day. An additional control using a 4 wt% PEG-OH polymer solution was peformed also showing limited solubility. In contrast, BrdU was mostly dissoluted in *star*-PEG_{113}-PPS_x hydrogel after simple vortexing for one minute (Figures 3b and 3c). *Star*-PEG-PPS hydrogel loaded with BrdU was injected directly in the wound bed (Figure 3d). To estimate the release of BrdU from *star*-PEG_{113}-PPS_x hydrogel, we first evaluated the *in vitro* daily release of BrdU from *star*-PEG_{113}-PPS_5 hydrogel and confirmed the sustained release imparted by the hydrogel carrier for at least one week (Figure 3e). During wound healing, collective migration of cells is primarily wound directed [35], so any diffusion of BrdU from *star*-PEG-PPS hydrogel would allow proliferating cells at wound periphery or beyond to uptake BrdU. Hence, the skin area was divided into three regions, i.e., the center of the wound bed (region I), the granulation tissue close to the boundary of the wound (region II) and the unwounded tissue surrounding the wound (region III) (Figure 3f). We expect the length of the PPS block can modulate the retention of the drug with in the wound, with longer blocks leading to increased retention. To account for the differences in cell proliferation in different wounds, another general proliferating cell marker, Ki-67, was used to gauge such difference and to normalize BrdU+ cells in the analysis of BrdU diffusion. The number of normalized proliferating cells was greater within the granulation tissue (regions I and II) and smaller in un-injured skin (region III)., *Star*-PEG_{113}-*b*-PPS_5 had significantly more normalized BrdU+ signals in the center of wound (region I) than *star*-PEG_{113}-*b*-$PPS_{2.5}$ at both day 3 and day 7 (Figure 3g). This evidence supports our hypothesis that a longer hydrophobic block enhances retention of hydrophobes, even in the presence of

aggressive cell infiltrations after injury. Noticeably, *star*-PEG-PPS hydrogel allowed for a z-directional (i.e., in various depths) BrdU uptake by cells, confirming the three-dimensional structure of the hydrogel for days at the wound bed for effective hydrophobe delivery from a scaffold.

Delivery of paradoxical MAPK activation via a hydrophobic BRAF inhibitor promotes wound closure

Vemurafenib (VEM) is a BRAF inhibitor that induces paradoxical mitogen-activated protein kinases (MAPK) activation and leads to enhanced keratynocyte proliferation and wound ehanced closure[21]. VEM is notoriously difficult to dissolve in an aqueous medium. Currently, either crystalline formulation or microprecipitated-bulk-powder formulation are given to patients for oral administration in clinical trials[36]. Vemurafenib dissolved in organic mediums for topical application could cause skin irritation and other side effects. As a first demonstration, we tested the efficacy of *star*-PEG_{113}-*b*-PPS_5 to load and deliver VEM in the repair of cutaneous wounds. Although we have previously demostrated VEM as a slurry in DMSO effectively promoted skin healing when administered three doses on days 0, 2, and 4, each containing 2 mg per wound[34], we hypothesized delivering a much lower dosage of solublized VEM within *star*-PEG-PPS hydrogels could achive similar or improved wound closure due to better drug dissolution, retention at the wound, and the mechanical/structural support provided by the scaffold. VEM was solubilized within 4 w/v% *star*-PEG_{113}-b-PPS_5 networks (Fig. 2b) and delivered to wound beds at a dose of 150 μg per wound. At first examination, VEM delivered in either DMSO or *star*-PEG-PPS resulted in complete re-epithelization (Figure 4a). Upon closer examination the wounds treated with *star*-PEG-PPS + VEM resulted in increased tissue volumes in both the demis and epidermis layers, showing improved tissue organization (Figure 4 a,b). Gross examination and quantification of the epithelium confirmed that the wound was closed by day 14 for DMSO + VEM and *star*-PEG-PPS + VEM treated wounds (Figure 4c). VEM enhances wound healing and tissue repair by causing the paradoxical activation of MAPK in keratinocytes, which leads to enhance proliferation of these cells. VEM delivered in *star*-PEG-PPS hydrogel led to increased phosphorylation of extracellular signal-regulated kinase (p-Erk) and cell proliferation (ki-67 positive) compared to VEM delivered in DMSO and controls (Figure 4d, e, and Supplementary Figure S6). A stronger activation was observed in VEM-loaded *star*-PEG-PPS hydrogel treated wounds than VEM/DMSO solution treated wounds, even though 40-fold less VEM was dosed with a single administration of *star*-PEG-PPS hydrogel than the DMSO solution (150 μg total versus 2 mg/dose × 3 doses).

The differences in wound closure rates between *star*-PEG-PPS and *star*-PEG-PPS + VEM led us to investigate the tissue response to VEM more closely. We observed keratin-14^+ cells with stratified squamous morphology over the surface of both scaffolds (Figure 5 a); however, in *star*-PEG-PPS + VEM scaffolds the keratin-14+ layer was thicker (Figure 5a). For VEM treated wounds, Keratin-14+ cells were present in the stratifying epidermis, which extended beyond the basilar keratinocytes. This result was indicative of a hyperproliferative epidermis [37]. The Keratin-14+ layer was significantly thicker in VEM-loaded *star*-PEG-PPS scaffolds, achieving similar Keratin-14+ thickness to a normal skin adjacent to the wound. This evidence indicated of a normal epithelial regeneration over the wound beds

when treated with *star*-PEG-PPS + VEM. For wounds treated with merely *star*-PEG-PPS, only the basal keratinocytes are Keratin-14+. At 14 days, substantial vascularization with endothelial cells (PECAM+) and supporting pericyte (NG2+) were observed in VEM-treated wounds(Figure 5b). Compared to scaffolds without VEM, both PECAM+ and NG2+ signals were significantly higher for wounds administered with VEM-loaded *star*-PEG-PPS hydrogel.

Conclusions

Star-PEG-PPS scaffolds are amphiphilic self-assembling *star*-shaped block copolymer that can simultaneously serve as both the scaffold for tissue repair and the drug delivery depot for hydrophobes. This approach opens the door to the delivery of hydrophobic agents from an injectable hydrogel at a location without the use of organic solvents or precipitates. Because most drugs in the market and in development are hydrophobic small molecules *star*-PEG-PPS hydrogels are believed to be applicable for the delivery of a wide range of hydrophobes to treat a variety of diseases. We demonstrate *star*-PEG-PPS hydrogels can dissolute a variety of hydrophobes and retain them within the scaffold *in vivo*.

Injectable *star*-PEG-PPS scaffolds filled the entire wound beds and provided a structural support for cellular infiltration and tissue regeneration. Delivery of VEM, a BRAF inhibitor promoting paradoxical MAPK activation, from *star*-PEG-PPS scaffolds led to enhanced wound closure and the formation of higher ordered structures within the newly formed tissue. Importantly, this was made possible with a substantially reduced dose of VEM compared to delivery of VEM in an organic solution. The combination of injectability, robust mechanical stability, and ability to dissolve and deliver hydrophobic drugs from these star amphiphilic scaffolds enables novel uses of hydrophobic drug formulations in various tissue repair applications and beyond.

Supplementary Material

Refer to Web version on PubMed Central for supplementary material.

Acknowledgements

We thank Dr. Juanjuan Du and Dr. Donald R. Griffin for their suggestions in the techniques performed for the synthesis of PEG-PPS polymer. We would also like to thank the Dr. William Lowry's research group and the California NanoSystems Institute (CNSI) for letting us use their cryostat and microtome instruments. This project was supported by the NSF IGERT: Materials Creation Training Program (MCTP, SZ) - DGE-0654431, NIH grant R01HL110592 (TS), and National Institute of General Medical Sciences T32 GM067555–11 (RD).

References

[1]. Scott DE , Bayly AR , Abell C , Skidmore J , Small molecules, big targets: drug discovery faces the protein-protein interaction challenge, Nat Rev Drug Discov, (2016).

[2]. Ishikawa M , Hashimoto Y , Improvement in aqueous solubility in small molecule drug discovery programs by disruption of molecular planarity and symmetry, J Med Chem, 54 (2011)1539–1554.21344906

[3]. Zhang Y , Strehin I , Bedelbaeva K , Gourevitch D , Clark L , Leferovich J , Messersmith PB , Heber-Katz E , Drug-induced regeneration in adult mice, Sci Transl Med, 7 (2015) 290–292.

[4]. Williams HD , Trevaskis NL , Charman SA , Shanker RM , Charman WN , Pouton CW , Porter CJH , Strategies to Address Low Drug Solubility in Discovery and Development, Pharmacol Rev, 65 (2013) 315–499.23383426

[5]. Miura Y , Takenaka T , Toh K , Wu S , Nishihara H , Kano MR , Ino Y , Nomoto T , Matsumoto Y , Koyama H , Cabral H , Nishiyama N , Kataoka K , Cyclic RGD-linked polymeric micelles for targeted delivery of platinum anticancer drugs to glioblastoma through the blood-brain tumor barrier, ACS Nano, 7 (2013) 8583–8592.24028526

[6]. Trimaille T , Mondon K , Gurny R , Moller M , Novel polymeric micelles for hydrophobic drug delivery based on biodegradable poly(hexyl-substituted lactides), Int J Pharm, 319 (2006) 147–154.16713691

[7]. Zhang Y , Song W , Geng J , Chitgupi U , Unsal H , Federizon J , Rzayev J , Sukumaran DK , Alexandridis P , Lovell JF , Therapeutic surfactant-stripped frozen micelles, Nat Commun, 7 (2016) 11649.27193558

[8]. Martin-Banderas L , Duran-Lobato M , Munoz-Rubio I , Alvarez-Fuentes J , Fernandez-Arevalo M , Holgado MA , Functional PLGA NPs for oral drug delivery: recent strategies and developments, Mini Rev Med Chem, 13 (2013) 58–69.22974367

[9]. Kang YM , Kim GH , Kim JI , Kim DY , Lee BN , Yoon SM , Kim JH , Kim MS , In vivo efficacy of an intratumorally injected in situ-forming doxorubicin/poly(ethylene glycol)-b-polycaprolactone diblock copolymer, Biomaterials, 32 (2011) 4556–4564.21440935

[10]. Park JH , Kim HA , Lee M , Amphiphilic peptide carrier for the combined delivery of curcumin and plasmid DNA into the lungs, Biomaterials, 33 (2012) 6542–6550.22687757

[11]. Yu B , Kang SY , Akthakul A , Ramadurai N , Pilkenton M , Patel A , Nashat A , Anderson DG , Sakamoto FH , Gilchrest BA , Anderson RR , Langer R , An elastic second skin, Nat Mater, (2016).

[12]. Shimizu T , Kishida T , Hasegawa U , Ueda Y , Imanishi J , Yamagishi H , Akiyoshi K , Otsuji E , Mazda O , Nanogel DDS enables sustained release of IL-12 for tumor immunotherapy, Biochem Bioph Res Co, 367 (2008) 330–335.

[13]. Shinde U , Pokharkar S , Modani S , Design and evaluation of microemulsion gel system of nadifloxacin, Indian J Pharm Sci, 74 (2012) 237–247.23439454

[14]. Chen PC , Kohane DS , Park YJ , Bartlett RH , Langer R , Yang VC , Injectable microparticle-gel system for prolonged and localized lidocaine release. II. In vivo anesthetic effects, J Biomed Mater Res A, 70 (2004) 459–466.15293320

[15]. Qiao M , Chen D , Ma X , Liu Y , Injectable biodegradable temperature-responsive PLGA-PEG-PLGA copolymers: synthesis and effect of copolymer composition on the drug release from the copolymer-based hydrogels, Int J Pharm, 294 (2005) 103–112.15814234

[16]. Appel EA , Tibbitt MW , Webber MJ , Mattix BA , Veiseh O , Langer R , Selfassembled hydrogels utilizing polymer-nanoparticle interactions, Nat Commun, 6 (2015) 6295.25695516

[17]. Nakahata M , Takashima Y , Yamaguchi H , Harada A , Redox-responsive self-healing materials formed from host-guest polymers, Nat Commun, 2 (2011) 511.22027591

[18]. Cheng X , Jin Y , Sun T , Qi R , Li H , Fan W , An injectable, dual pH and oxidation-responsive supramolecular hydrogel for controlled dual drug delivery, Colloids Surf B Biointerfaces, 141 (2016) 44–52.26851440

[19]. Napoli A , Valentini M , Tirelli N , Muller M , Hubbell JA , Oxidation-responsive polymeric vesicles, Nat Mater, 3 (2004) 183–189.14991021

[20]. Zhang J , Tokatlian T , Zhong J , Ng QK , Patterson M , Lowry WE , Carmichael ST , Segura T , Physically associated synthetic hydrogels with long-term covalent stabilization for cell culture and stem cell transplantation, Adv Mater, 23 (2011) 5098–5103.21997799

[21]. Escuin-Ordinas H , Li SR , Xie MW , Sun L , Hugo W , Huang RR , Jiao J , de-Faria FM , Realegeno S , Krystofinski P , Azhdam A , Komenan SMD , Atefi M , Comin-Anduix B , Pellegrini M , Cochran AJ , Modlin RL , Herschman HR , Lo RS , McBride WH , Segura T , Ribas A , Cutaneous wound healing through paradoxical MAPK activation by BRAF inhibitors, Nature Communications, 7 (2016).

[22]. Zhang JJ , Tokatlian T , Zhong J , Ng QKT , Patterson M , Lowry WE , Carmichael ST , Segura T , Physically Associated Synthetic Hydrogels with Long-Term Covalent Stabilization for Cell Culture and Stem Cell Transplantation, Advanced Materials, 23 (2011) 5098–5103.21997799

[23]. Napoli A , Tirelli N , Wehrli E , Hubbell JA , Lyotropic behavior in water of amphiphilic ABA triblock copolymers based on poly(propylene sulfide) and poly(ethylene glycol), Langmuir, 18 (2002) 8324–8329.

[24]. Galiano RD , Michaels J.t. , Dobryansky M , Levine JP , Gurtner GC , Quantitative and reproducible murine model of excisional wound healing, Wound Repair Regen, 12 (2004) 485–492.15260814

[25]. Olsen BD , Kornfield JA , Tirrell DA , Yielding Behavior in Injectable Hydrogels from Telechelic Proteins, Macromolecules, 43 (2010) 9094–9099.21221427

[26]. Sen CK , Roy S , Redox signals in wound healing, Biochim Biophys Acta, 1780 (2008) 1348–1361.18249195

[27]. Kolaczkowska E , Kubes P , Neutrophil recruitment and function in health and inflammation, Nat Rev Immunol, 13 (2013) 159–175.23435331

[28]. Mittal M , Siddiqui MR , Tran K , Reddy SP , Malik AB , Reactive oxygen species in inflammation and tissue injury, Antioxid Redox Signal, 20 (2014) 1126–1167.23991888

[29]. Jun JI , Kim KH , Lau LF , The matricellular protein CCN1 mediates neutrophil efferocytosis in cutaneous wound healing, Nat Commun, 6 (2015) 7386.26077348

[30]. Lan CC , Wu CS , Huang SM , Wu IH , Chen GS , High-glucose environment enhanced oxidative stress and increased interleukin-8 secretion from keratinocytes: new insights into impaired diabetic wound healing, Diabetes, 62 (2013) 2530–2538.23423570

[31]. Malten KE , Denarend J , Topical Toxicity of Various Concentrations of Dmso Recorded with Impedance Measurements and Water-Vapor Loss Measurements - Recording of Skin Adaptation to Repeated Dmso Irritation, Contact Dermatitis, 4 (1978) 80–92.668341

[32]. Capriotti K , Capriotti JA , Dimethyl sulfoxide: history, chemistry, and clinical utility in dermatology, J Clin Aesthet Dermatol, 5 (2012) 24–26.

[33]. Chereddy KK , Vandermeulen G , Preat V , PLGA based drug delivery systems: Promising carriers for wound healing activity, Wound Repair Regen, 24 (2016) 223–236.26749322

[34]. Oba Y , and Poulson SR , Octanol-water partition coefficients vs. pH for fluorescent dye tracers, and implications for hydrologic tracer tests, Geochemical Journal, 46 (2012) 517–520.

[35]. Chapnick DA , Liu XD , Leader cell positioning drives wound-directed collective migration in TGF beta-stimulated epithelial sheets, Mol Biol Cell, 25 (2014) 1586–1593.24623725

[36]. Flaherty KT , Puzanov I , Kim KB , Ribas A , McArthur GA , Sosman JA , O'Dwyer PJ , Lee RJ , Grippo JF , Nolop K , Chapman PB , Inhibition of mutated, activated BRAF in metastatic melanoma, N Engl J Med, 363 (2010) 809–819.20818844

[37]. Ota T , Takekoshi S , Takagi T , Kitatani K , Toriumi K , Kojima T , Kato M , Ikoma N , Mabuchi T , Ozawa A , Notch signaling may be involved in the abnormal differentiation of epidermal keratinocytes in psoriasis, Acta Histochem Cytochem, 47 (2014) 175–183.25392571

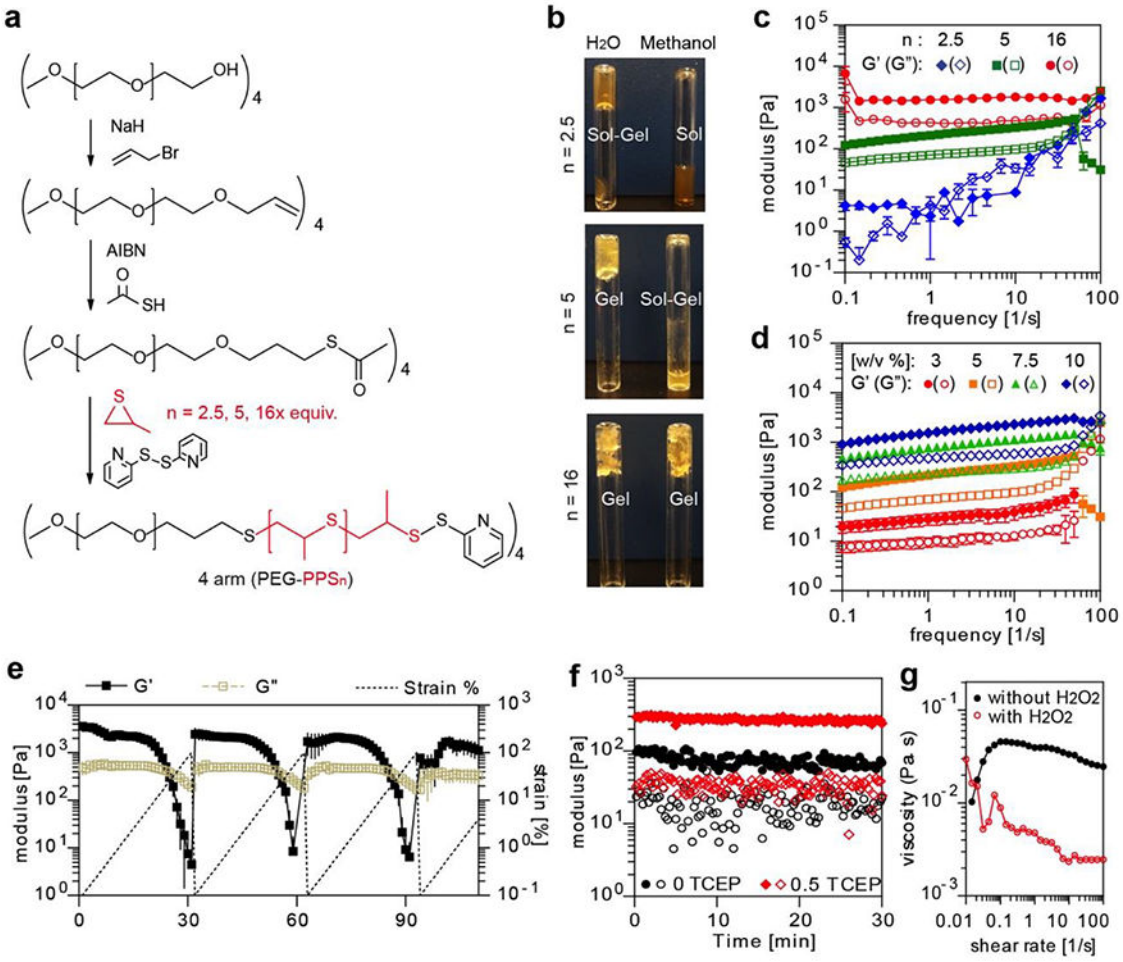

Figure 1.

The viscoelasticity of the *star*-PEG-PPS famility in different solvents, concentrations, reduction, and oxidation environments. **a**. Synthesis route of 4-arm *star*-PEG_{113}-PPS_5. **b**. When resuspended in water at 10 w/v%, *star*-PEG-$PPS_{2.5}$ exhibited sol-gel transition, *star*-PEG-PPS_5 was fully hydrated, and *star*-PEG-PPS_{16} was partially hydrated with pockets of water not absorbed. When resuspended in methanol, *star*-PEG-$PPS_{2.5}$ flowed under gravity, *star*-PEG-PPS_5 exhibited sol-gel transitioning, and *star*-PEG-PPS_{16} was hydrated as hydrogel. **c**. The rhelogical property of 10 w/v % *star*-PEG-$PPS_{2.5}$ (in water), *star*-PEG-PPS_5 (in water) and *star*-PEG-PPS_{16} (in methanol). **d**. The rheological moduli of *star*-PEG-PPS_5 hydrogels of different concentration under 1% strain. **e**. The yielding and healing behaviors of 10 w/v% *star*-PEG-PPS_5 in aqueous environment. **f**. Reducing agent TCEP increased the stiffness of *star*-PEG-PPS_5 hydrogel (n(Polymer arm) : n(TCEP) = 1 : 0.5). Polymers were at 4.75 w/v%, and measured under 1% strain. **g**. Hydrogen peroxide (5 v/v%) decreases the viscosity of *star*-PEG-PPS_5 (3 w/v%).

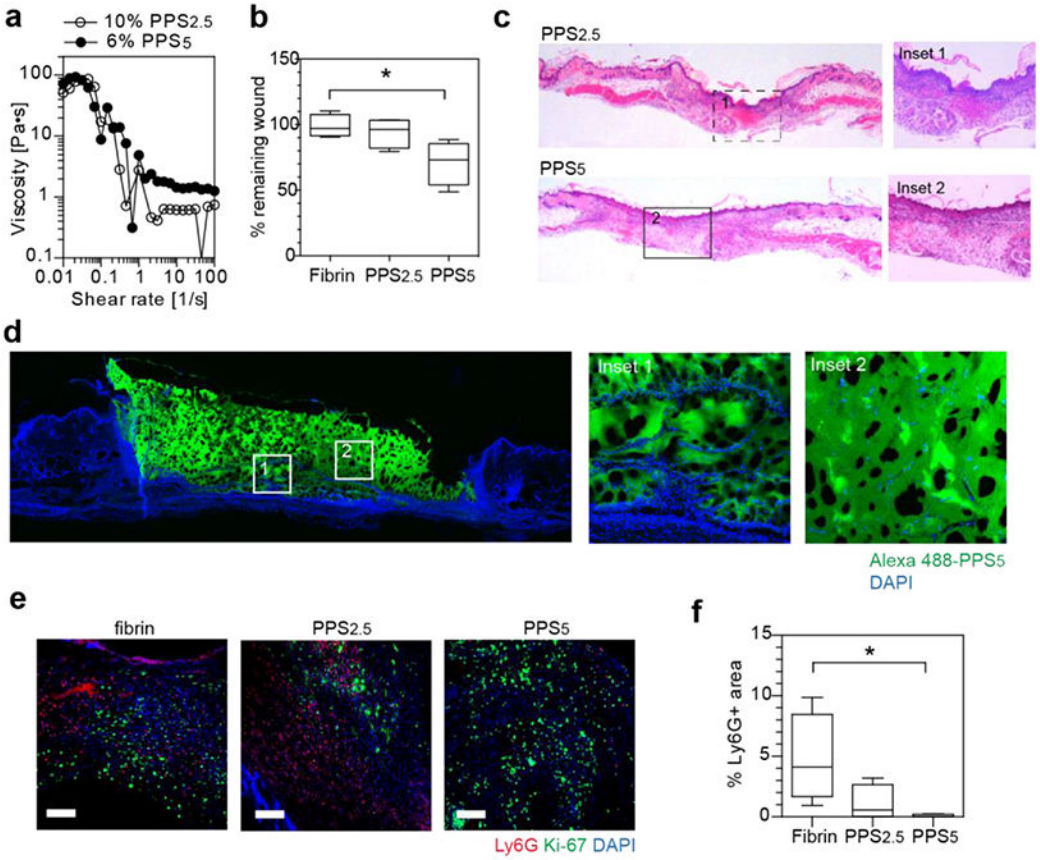

Figure 2.

Injectable *star*-PEG-PPS hydrogels as biocompatible cutaneous wound scaffolds. **a**. *star*-PEG-PPS_5 (6 w/v% in PBS) and *star*-PEG-$PPS_{2.5}$ (10 w/v% in PBS) showed a similar viscosity and injectability. **b**. Wound closure comparision at day 3 in mouse splinted dermal excisional wound healing model among fibrin matrix (10 mg/mL fibrinogen), 10 w/v% *star*-PEG-$PPS_{2.5}$, and 6 w/v% *star*-PEG-PPS_5. **c**. H&E staining of day 7 mouse splinted dermal wounds, full length and inset showing wound bed center. **d**. Fluorescent imaging of day 7 mouse splinted dermal wound filled with Alexa 488-labeled *star*-PEG-PPS_5. **e**. Immunohistochemical staining of day 7 neutrophil marker (Ly6G, red), proliferating cells (Ki-67, green), and nuclei (DAPI, blue) in wound beds dressed with fibrin matrix (10 mg/mL fibrinogen), 10 w/v% *star*-PEG-$PPS_{2.5}$, or 6 w/v% *star*-PEG-PPS_5. **f**. Quantification of images in e for positive Ly6G area. (n=4; one-way ANOVA, non-parametric, Tukey's post test; Scale bar = 20 μm).

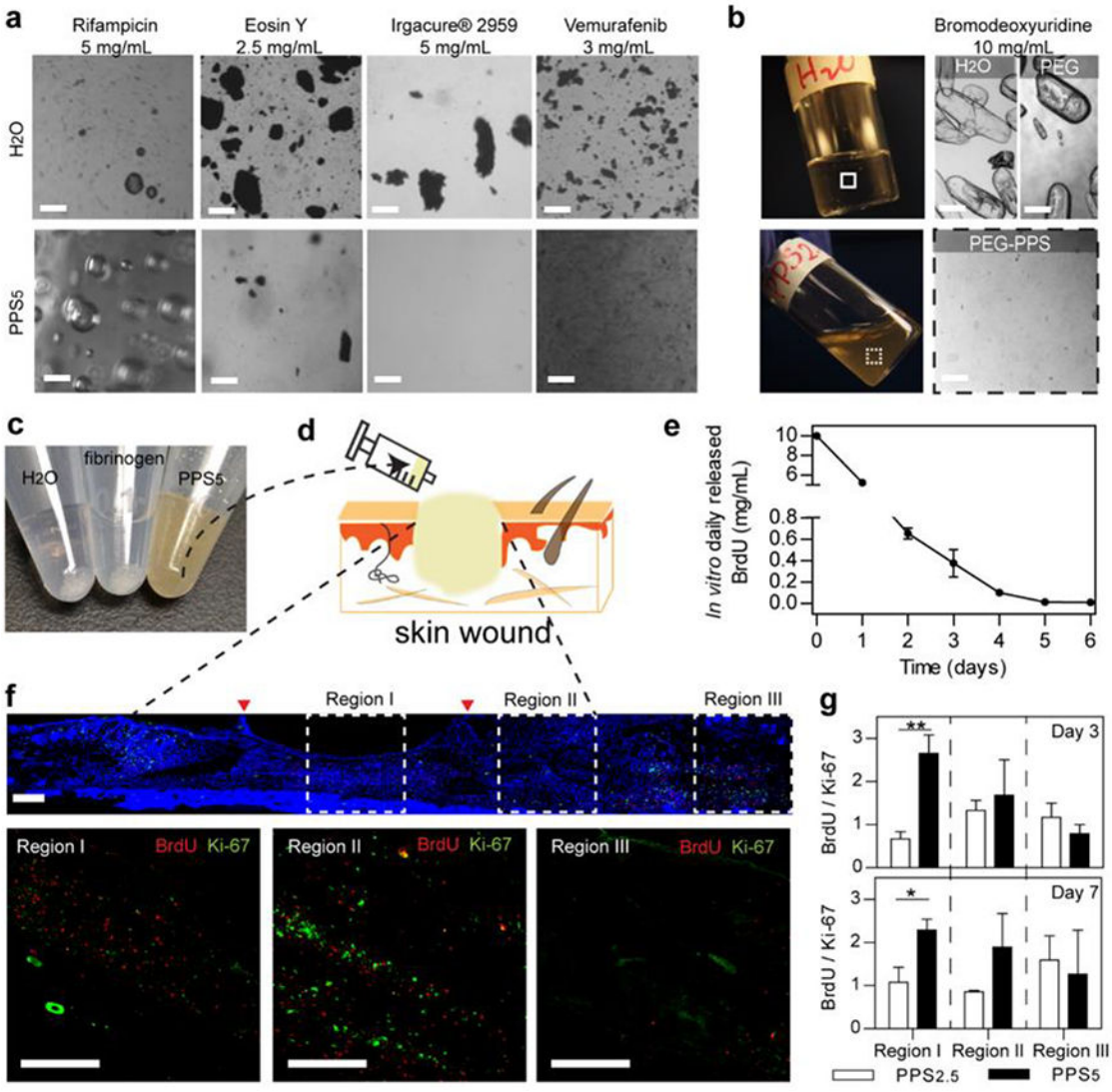

Figure 3.

Solubilization of hydrophobes and delivery of BrdU via *star*-PEG-PPS hydrogel scaffolds as mouse dermal wound dressings for 7-day retention. **a**. Dissolution of different hydrophobic molecules in water and in 4 w/v% *star*-PEG-PPS_5 aqueous suspension. **b**. Top, BrdU in water or 4wt % PEG-OH polymer solution at room temperature, after 30 minutes of vortexing; bottom, BrdU in 10 w/v% aqueous *star*-PEG-$PPS_{2.5}$ network. **c**. BrdU (20 mg/mL) suspended in water (left), fibrinogen aqueous solution (middle), and *star*-PEG-PPS_5 (right). **d**. Schematic of injectable scaffold delivering hydrophobic BrdU at wound beds. **e**. *In vitro* release of BrdU from *star*-PEG-PPS_5. **f**. Representative full-length wound scan of BrdU (red), Ki-67 (green) and DAPI (blue) at day 3 with insets indicating regions at the center of wound beds (I), the granulation tissue (II), and the skin tissues outside of wound (III). **g**. Quantifications of normalized BrdU+ over Ki-67+ in Regions I, II, and III comparing between 6 w/v% *star*-PEG-PPS_5 and 10 w/v% *star*-PEG-$PPS_{2.5}$. (e). One-way ANOVA, * $p < 0.05$, ** $p < 0.01$). Size bars are 100μm.

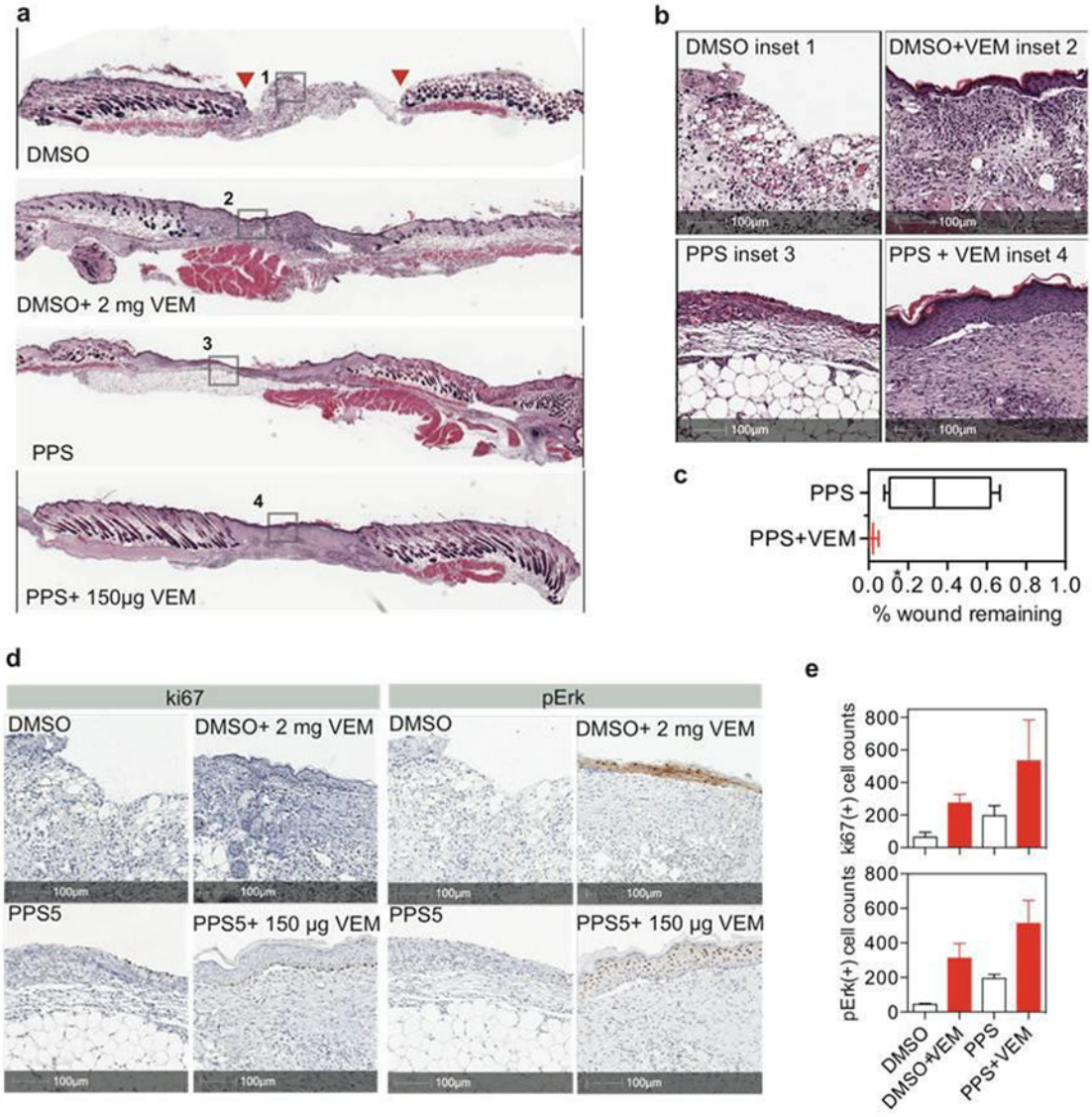

Figure 4.

Star-PEG$_{113}$-PPS$_5$ hydrogel (PPS) delivering solubilized vemurafenib (VEM) as a scaffold at mouse dermal wounds. **a**.**b**. Full-wound scan (a) and inset (b) of H&E stained wounds at 14 days that were dressed at day 0 prior to splinting with (1) DMSO, (2) 2 mg VEM dissolved in DMSO at 0.1 mg/μL, and redosed at day 2 and day 4 for a total of three doses, (3) 4 w/v% *star*-PEG$_{113}$-PPS$_5$ hydrogel (PPS), or (4) 150 μg VEM dissolved in 4 w/v% *star*-PEG$_{113}$-PPS$_5$ hydrogel (PPS). **c**. Percent of wound remaining at day 14. **d**. **e**. Staining and quantification of ki67 and pErk positive cells at 14 days post treatment.

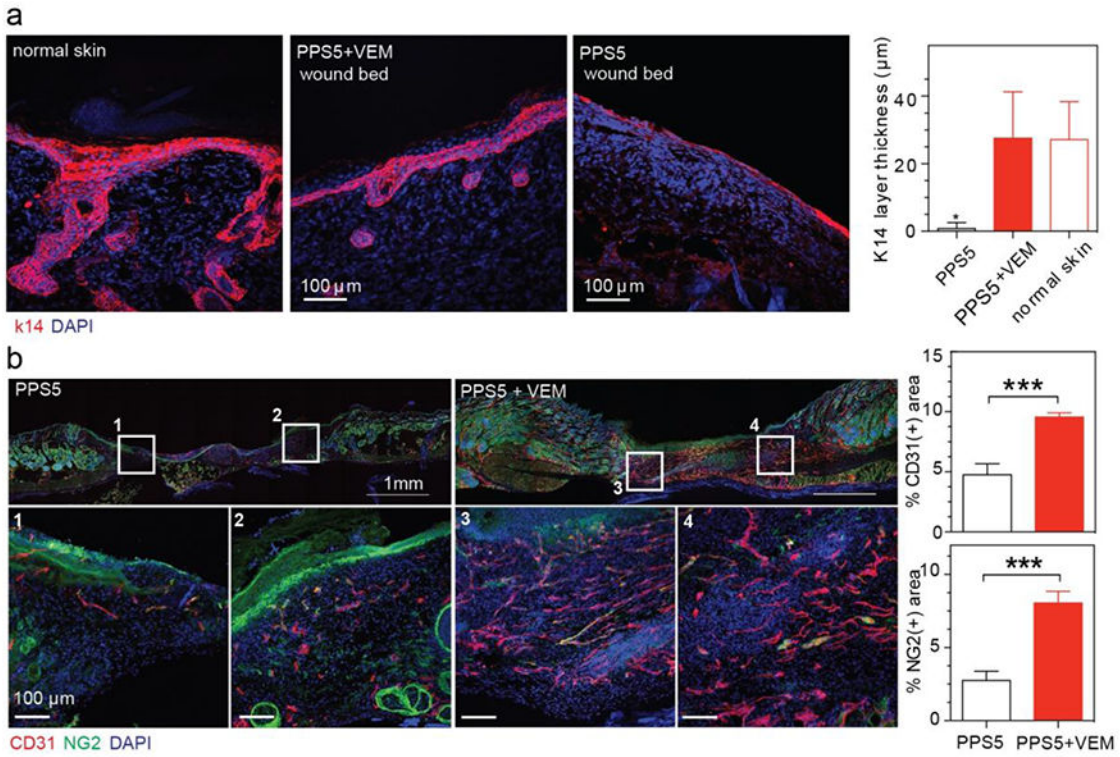

Figure 5.

Star-PEG$_{113}$-PPS$_5$ hydrogel (PPS) delivering solubilized vemurafenib (VEM) therapeutically restores stratyfing epidermis at 14 days. **a**. Microscopic analysis and quantification of k14 layer thickness. b. Microscopic analysis and quantification of angiogenesis (CD31) and pericyte coverage (NG2) of wounds with different treatments.